Accelerated Publications

Cocrystal Structure of Protein Farnesyltransferase Complexed with a Farnesyl Diphosphate Substrate[†,‡]

Stephen B. Long,[§] Patrick J. Casey,[§,||] and Lorena S. Beese*[,§]

Department of Biochemistry and Department of Pharmacology and Cancer Biology, Duke University Medical Center, Durham, North Carolina 27710

Received March 27, 1998; Revised Manuscript Received May 15, 1998

ABSTRACT: Protein farnesyltransferase (FTase) catalyzes the transfer of the hydrophobic farnesyl group from farnesyl diphosphate (FPP) to cellular proteins such as Ras at a cysteine residue near their carboxy-terminus. This process is necessary for the subcellular localization of these proteins to the plasma membrane and is required for the transforming activity of oncogenic variants of Ras, making FTase a prime target for anticancer therapeutics. The high-resolution crystal structure of rat FTase was recently determined, and we present here the X-ray crystal structure of the first complex of FTase with a FPP substrate bound at the active site. The isoprenoid moiety of FPP binds in an extended conformation in a hydrophobic cavity of the β subunit of the FTase enzyme, and the diphosphate moiety binds to a positively charged cleft at the top of this cavity near the subunit interface. The observed location of the FPP molecule is consistent with mutagenesis data. This binary complex of FTase with FPP leads us to suggest a "molecular ruler" hypothesis for isoprenoid substrate specificity, where the depth of the hydrophobic binding cavity acts as a ruler discriminating between isoprenoids of differing lengths. Although other length isoprenoids may bind in the cavity, only the 15-carbon farnesyl moiety binds with its C1 atom in register with a catalytic zinc ion as required for efficient transfer to the Ras substrate.

Protein farnesyltransferase (FTase)[1] catalyzes the addition of the hydrophobic farnesyl isoprenoid to the thiol of a cysteine residue near the carboxy terminus of protein acceptors such as Ras, thereby affixing these proteins to the cell membrane. The enzyme uses the 15-carbon farnesyl diphosphate (FPP) as the prenyl donor in this reaction. FTase modifies protein substrates with a carboxy-terminal "CaaX" sequence motif, where C is the cysteine at which the iosprenoid thioether linkage is formed, "a" is generally an aliphatic amino acid, and X, the carboxy-terminal residue, is typically methionine, and less frequently serine, or glutamine *(1*−*3)*. Since attachment of the farnesyl group to oncogenic variants of Ras is essential for their transforming effect, FTase is a prime target for anticancer drugs. Specific inhibitors of FTase have been shown to reverse the cellular transformation induced by these forms of Ras (*4*−*6*). A better understanding of the structural and mechanistic details of the reaction catalyzed by FTase should provide valuable information for the design and evaluation of new or improved inhibitors.

FTase is a heterodimer consisting of 48-kDa (α) and 46-kDa (β) subunits; the α subunit also forms a component of the closely related enzyme, protein geranylgeranyltransferase type I (GGTase-I) (*7, 8*). GGTase-I transfers a 20-carbon isoprenoid from geranylgeranyl diphosphate (GGPP) to the cysteine residue of proteins ending in a slightly different "CaaX" motif where X is typically leucine for the GGTase substrate (*1*−*3, 9*). FTase has been shown to contain one atom of zinc per protein dimer, which is absolutely required for catalytic activity and dramatically enhances peptide but not FPP binding (*10, 11*). Many lines of experimental evidence indicate that the zinc is directly involved in catalysis (*8, 10, 12*−*14*) including spectroscopic experiments on Co^{2+}-substituted FTase which suggest that the cysteine thiol of the CaaX substrate directly coordinates the zinc in a ternary complex (*14*). The detailed chemical mechanism by which FTase transfers the farnesyl moiety from FPP to the cysteine thiol of the protein substrate to form a thioether is not yet clear. Studies on Co^{2+}-substituted rat FTase support a

[†] This work was supported by grants from the NIH (GM52382), Searle Scholar Foundation, and Schering-Plough Research Institute to L.S.B. and by NIH Grant GM46372 to P.J.C.

[‡] The coordinates have been deposited at the Brookhaven Protein Data Bank (ID code: 1FT2).

* To whom correspondence should be addressed: Department of Biochemistry, Box 3711, Duke University Medical Center, Durham, NC 27710. Tel: 919-681-5267. Fax: 919-684-8885. E-mail: lsb@bchm.biochem.duke.edu.

[§] Department of Biochemistry, Duke University Medical Center.

[||] Department of Pharmacology and Cancer Biology, Duke University Medical Center.

[1] Abbreviations: FTase, protein farnesyltransferase; FPP, farnesyl diphosphate; GGPP, geranylgeranyl diphosphate; CaaX, a sequence motif consisting of an invariant cysteine residue fourth from the carboxy terminus; apo FTase, protein farnesyltransferase with zinc but without substrates; IC_{50}, concentration of inhibitor which causes a 50% decrease in catalytic activity.

S0006-2960(98)00708-9 CCC: $15.00
Published on Web 06/17/1998

nucleophilic mechanism of farnesyl transfer in which the zinc ion activates the cysteine thiol of the protein substrate for attack at C1 of FPP (*14*). An electrophilic component to the mechanism has also been proposed on the basis of experiments with the yeast enzyme using a series of fluoro-substituted FPP analogues and other compounds designed to mimic a transition state postulated to occur in an electrophilic alkylation mechanism (*15, 16*). Further studies are required to establish the exact chemical mechanism for prenyl transfer.

Steady-state kinetic analysis of FTase initially suggested that the reaction follows a random-ordered sequential reaction pathway (*17*). However, further investigation of the reaction pathway by steady-state isotope trapping experiments (*18*) and pre-steady-state kinetic analysis (*19*) indicates that the reaction proceeds via a functionally ordered mechanism in which FPP binds first to form a binary complex, followed by binding of the protein substrate. Pre-steady-state kinetic analysis (*19*) suggests that the rate-limiting step in the reaction follows prenyl transfer and may be the release of the prenylated product. Furthermore, this product release step is enhanced by the binding of an additional substrate molecule, with FPP being the most effective substrate in this regard (*20*).

The X-ray crystal structure of heterodimeric rat FTase was recently determined at 2.25 Å resolution (*21*). The α subunit was folded into a crescent-shaped domain composed of seven successive pairs of coiled-coils or "helical hairpins" that envelopes part of the β subunit. The β subunit was folded into an α−α barrel domain consisting of a core of six parallel helices forming the inner portion of the barrel and six peripheral helices. One end of the barrel was blocked, while the other end was solvent accessible. The catalytic zinc ion bound at the top of the barrel near the subunit interface, marking the active site. The side chains of Cys 299β, Asp 297β, and His 362β observed to coordinate the zinc ion subsequently have been confirmed by site-directed mutagenesis to be zinc ligands (*22, 23*). A striking feature of the β subunit was a deep, funnel-shaped cavity in the center of the α−α barrel lined with 10 highly conserved aromatic residues. This hydrophobic cavity was hypothesized to bind the farnesyl moiety of FPP with the required specificity. A shallow hydrophilic cleft in the β subunit ran parallel to the rim of the α−α barrel near the subunit interface and intersected the hydrophobic cavity at the catalytic zinc ion. In the crystal structure, nine carboxy-terminal residues (Ala^9-Val^8-Thr^7-Ser^6-Asp^5-Pro^4-Ala^3-Thr^2-Asp^1-COOH) of a second β subunit, not part of the dimer but adjacent in the crystal lattice, were found to bind in this hydrophilic cleft. Although not common, such intersubunit peptide crossover has been observed previously in other crystal structures. Several lines of evidence suggested that these carboxy-terminal nine residues might mimic some aspects of normal CaaX peptide binding (*21*). Most significantly, the position of the fourth residue from the carboxy terminus, corresponding to the cysteine to be farnesylated in the CaaX motif, was in register with the zinc ion and was adjacent to the predicted position of the FPP α phosphate. The thiol of a cysteine modeled at this position could coordinate to the observed zinc ion.

Cross-linking studies provided the initial evidence that the binding sites for both peptide and isoprenoid substrates reside primarily on the β subunit of FTase (*24*−*27*), and this assignment has been further supported by mutagenesis of conserved residues of the β subunit in the yeast and human enzyme (*22, 28*). The primary localization of substrate binding to their distinct β subunits is consistent with the different specificities of FTase and GGTase-I since, as noted above, the two enzymes share an identical α subunit; the ability of FTase to distinguish its 15-carbon FPP substrate, from the 20-carbon substrate used by GGTase (geranylgeranyl diphosphate, or GGPP), has been hypothesized to be based on the depth of the prominent hydrophobic cavity revealed in the crystal structure of FTase (*21*). Structural and mutagenesis studies of farnesyl diphosphate synthase (FPS), which catalyzes the synthesis of FPP, show that the length of the isoprenoid product synthesized by the enzyme is governed by the depth of a hydrophobic pocket in which it binds (*29*). Protein prenyltransferases may use an analogous mechanism to identify their isoprenoid substrates.

Here we report the first X-ray crystal structure of FTase with its natural substrate FPP. This complex defines the FPP binding site, confirming the originally postulated location and providing further support for the "molecular ruler" hypothesis for prenyl substrate specificity.

EXPERIMENTAL PROCEDURES

Sample Preparation and Cocrystallization. Recombinant rat FTase was produced using an Sf9 cell overexpression system, purified as described previously (*11*), and concentrated to 16 mg/mL in 20 mM Tris-HCl buffer (pH 7.7) containing 20 mM KCl, 10 μM ZnCl, and 1 mM dithiothreitol. FPP (American Radiolabeled Chemicals) was dissolved in 20 mM Tris-HCl buffer (pH 7.7) containing 0.6% (w/v) octyl β-D-glucopyranoside (Fluka), combined with FTase (final concentrations of 1 mM FPP and 0.14 mM FTase), and incubated on ice for 30 min prior to crystallization. Cocrystals were grown at 17 °C from hanging drops containing the FTase-FPP solution and reservoir solution [15% (w/v) PEG-8000, 200 mM ammonium acetate (pH 7.0), 100 mM imidazole−malic acid (pH 7.0), 10 mM dithiothreitol] and equilibrated against the reservoir solution by vapor diffusion.

Cocrystals were transferred stepwise into a cryoprotectant containing 43% (w/v) PEG-8000, 20% sucrose (w/v), 200 mM ammonium acetate, 100 mM imidazole−malic acid (pH 7.0), 20 mM KCl, 20 mM Tris-HCl (pH 7.7), 10 mM dithiothreitol, 0.003% (w/v) octyl β-D-glucopyranoside, and 0.1 mM FPP. Cocrystals were equilibrated in the cryoprotectant solution for 18 h and cryocooled in liquid nitrogen.

Crystallographic Data Collection and Model Refinement. Diffraction data were measured at 98 K with an R-axis II image plate system (Molecular Structure Corp., MSC) mounted on a Rigaku RU-200 rotating anode generator with double mirror optics (MSC). Data reduction and scaling were done using the DENZO and SCALEPACK programs (*30*).

Both the FTase−FPP cocrystals and apo FTase crystals belong to the spacegroup $P6_5$ with unit cell dimensions $a = b = 167$ Å. The c unit cell dimension is 99 Å for the cocrystals, approximately 1 Å larger than observed for crystals of apo FTase. Phase calculation and model refinement were done in X-PLOR (*31*) utilizing a bulk solvent correction (*32*). The 2.25 Å resolution refined structure of

Table 1: Summary of X-Ray Data Collection and Crystallographic Refinement

X-ray data collection		refinement[a]	
resolution range (Å)	35−3.4	resolution range (Å)	35−3.4
no. of observations	42609	no. of reflections[c]	17125
no. of unique reflections	17125	completeness (%)[c]	79.4 (58.1)[b]
R_{sym} (%)	5.3	R (%)	22.0
completeness (%)	79.4 (58.1)[b]	R_{free} (%)[d]	26.8
		no. of non-hydrogen atoms	5865
		rms deviation from ideal values	
		bond length (Å)	0.009
		bond angle (deg)	1.73

[a] Using the X-PLOR program package (*31*). [b] Denotes completeness in the highest resolution shell. [c] Using all reflections. [d] To prevent bias in the calculation, the reflections used to compute R_{free} (5% of the total) were drawn from the set used to compute R_{free} in the model refinement of apo FTase (*21*).

apo FTase with the water molecules omitted was used as a starting model (*21*). The structure was visualized and modified with the program O (*33*). Electron density maps were calculated using the CCP4 suite of programs (*34*). Table 1 contains a summary of the diffraction data and refinement statistics for the binary complex.

RESULTS

Initial difference electron density maps ($F_{FTase-FPP} - F_c$) showed strong positive density (5σ over background) in the hydrophobic cavity of the α−α barrel of the β subunit. No density was observed for 15 carboxy-terminal residues of the β subunit. The initial maps also indicated several side-chain rearrangements and the motion of a short loop connecting helices 12β and 13β (*21*). Model adjustment followed by crystallographic refinement increased the intensity and connectivity of the density in the active site region. Farnesyl diphosphate (FPP) was fit into this density and the model refined. The final $F_{FTase-FPP} - F_c$ difference electron density map calculated with the FPP molecule omitted from the phase calculation is shown in Figure 1.

The FPP molecule binds to the β subunit with its isoprenoid moiety along one side of the funnel-shaped, hydrophobic cavity of the α−α barrel as originally hypothesized on the basis of the apoenzyme crystal structure (*21*) (Figures 2−4). Highly conserved aromatic residues Trp 303β, Tyr 251β, Trp 102β, Tyr 205β, and Tyr 200α form hydrophobic interactions with the isoprenoid (Figure 3). Strictly conserved Arg 202β, which adopts a different side-chain conformation from the apo FTase structure, also forms a hydrophobic interaction with the isoprenoid. Arg 202β is further stabilized by Asp 200β and a hydrophobic interaction with Met 193β. This methionine adopts a different conformation in the binary complex to accommodate the new position of Arg 202β. In addition, two residues on helix 9β, conserved Cys 254β and Gly 250β, also contribute to the isoprenoid binding site (Figure 3).

The location of the zinc ion and its coordination by the side chains of Cys 299β, Asp 297β, and His 362β are unchanged from the apo FTase crystal structure within the error of the coordinates. The diphosphate moiety of the FPP molecule binds in a positively charged cleft near the subunit interface and is adjacent to the catalytic zinc ion (Figures 2 and 3). Although with a 3.4 Å resolution structure it is not possible to determine unambiguously which residues form hydrogen bonds, the diphosphate moiety of the FPP molecule is within 3.5 Å of the β subunit residues His 248β, Arg 291β,

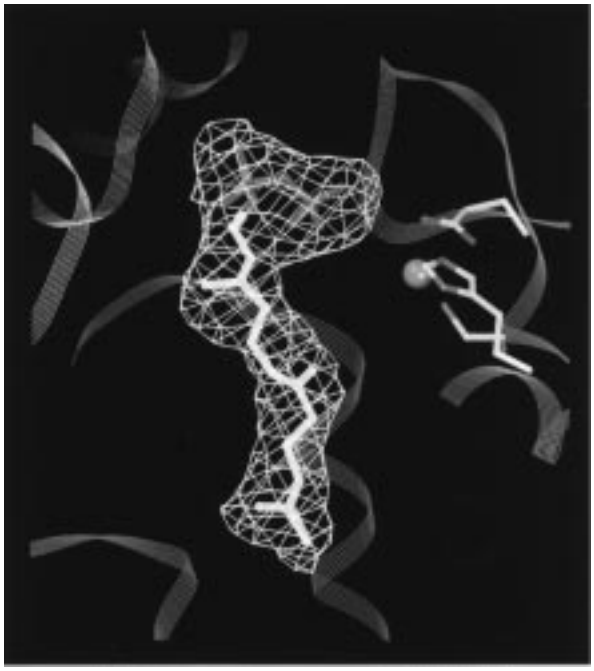

FIGURE 1: FPP superimposed on an omit electron density map calculated from 3.4 to 35 Å resolution using Fourier coefficients $(F_{FTase-FPP} - F_c)\alpha_{calc}$ with FPP omitted from the calculation. A 3σ contour is shown. Portions of the α and β subunits of FTase are shown as ribbon representations colored in orange and blue, respectively. The catalytic zinc ion, shown as a pink sphere, is adjacent to the FPP molecule and is coordinated by Asp 297β, Cys 299β, and His 362β. This figure was produced with the program O (*33*).

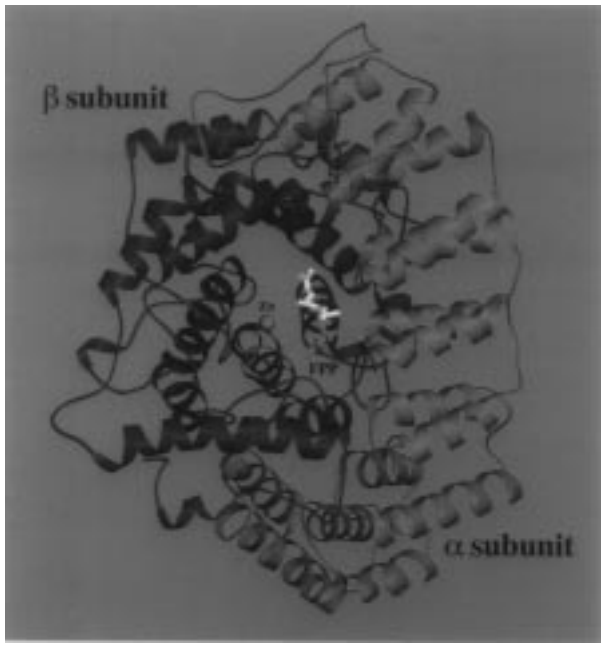

FIGURE 2: Overview of FTase with bound FPP. The FPP molecule, shown as a stick representation, binds with its isoprenoid moiety in the funnel-shaped, hydrophobic cavity inside the α−α barrel of the β subunit. Its diphosphate moiety binds in a positively charged cleft near the subunit interface and is adjacent to the catalytic zinc ion, which is shown as a sphere. This figure was produced with RIBBONS (*46*).

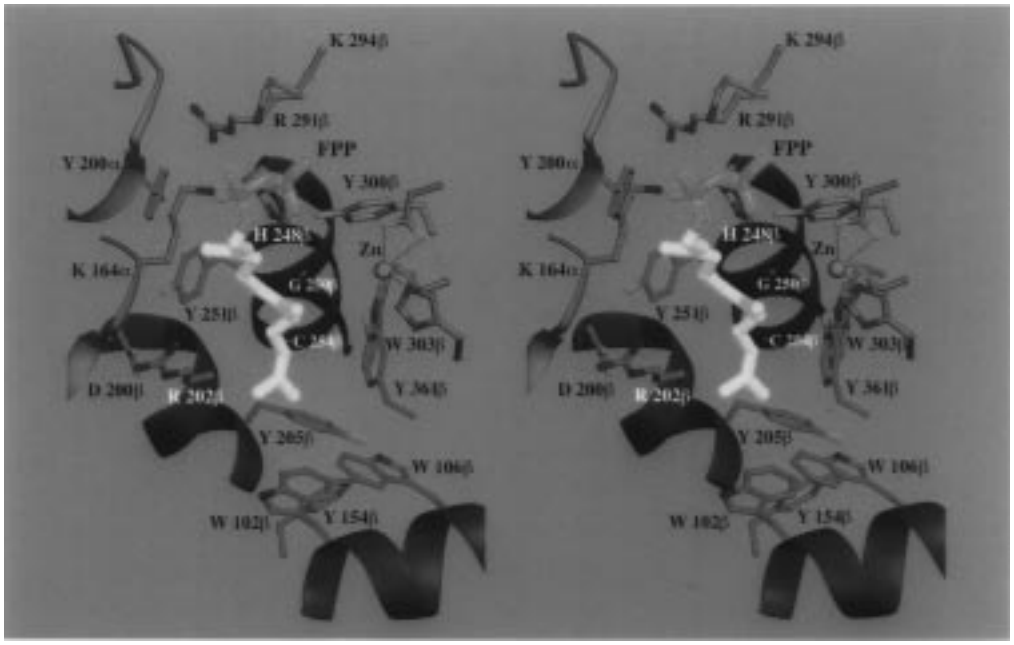

FIGURE 3: Stereoview of the active site with FPP bound. Portions of the α and *β* subunits are drawn as ribbons in red and blue, respectively. The isoprenoid moiety of the FPP molecule binds to the hydrophobic cavity inside the α−α barrel of the *β* subunit. Residues colored in green line this hydrophobic cavity. The diphosphate group of the FPP molecule binds in a positively charged cleft near the subunit interface formed by residues colored in pink and is adjacent to the catalytic zinc ion whose ligands are colored in gray. Confirming the observed location of the FPP molecule, mutation of *β* subunit residues His 248*β*, Arg 291*β*, Lys 294*β*, Tyr 300*β*, or Trp 303*β* results in an increase in $K_{d(FPP)}$ (*22*). Lys 164α, which when mutated to Asn dramatically reduces catalytic turnover (*36*), is in close proximity to the C1 atom of the FPP molecule and may be directly involved in catalysis. This figure was generated with RIBBONS (*46*).

and Tyr 300*β*—all of which are strictly conserved in prenyltransferase enzymes—and lies directly above helix 9*β* whose N-terminal positive dipole contributes to the strong positive charge of this pocket. Invariant residues Lys 164α and Lys 294*β* are also within hydrogen-bonding distance to the α and *β* phosphate groups (Figure 3), although the side chain of Lys 294*β* is not well ordered in the electron density.

A striking difference between the structures of apo FTase and the FPP−FTase complex is that the nine carboxy-terminal residues of the *β* subunit that in apo FTase crystals bind in the hydrophilic cleft of a symmetry-related *β* subunit are displaced by the binding of FPP. These residues were proposed to mimic some aspects of CaaX peptide binding. A total of 15 carboxy-terminal residues of the *β* subunit are disordered in the binary complex. Displacement of these residues is accompanied by the motion of the loop connecting helices 12*β* and 13*β* of the *β* subunit. The apex of the loop (at Ser 357*β*) is approximately 3.5 Å from its position in the apo FTase structure. This loop is in contact with the carboxy-terminal residues of the *β* subunit in the apo FTase structure. The position of the loop observed in the FPP−FTase complex would sterically clash with the carboxy-terminal residues of the *β* subunit observed in the apo FTase structure, suggesting that the repositioning of the loop is the result of the displacement of these carboxyl-terminal residues and not a direct consequence of binding FPP.

Overall, however, the apo FTase structure and the FPP−FTase structures are very similar (0.2 Å rms deviation in C_α positions), showing few conformational changes due to FPP binding. In the active site region, the differences between the apo crystal structure and the FPP binary complex are primarily limited to the movement of the side chains of Arg 202*β* and Met 193*β*. Fluorescence (*19*) and CD studies (*35*) have led to the proposal that FTase undergoes a dramatic conformational change upon binding FPP. The observed spectroscopic changes upon binding FPP may in part be accounted for by displacement of bound solvent in the isoprenoid binding cavity, in addition to subtle repositioning of any of the 10 aromatic residues which line the α−α barrel of the *β* subunit upon FPP binding.

DISCUSSION

Mutagenesis Data Are Consistent with the Observed FPP Binding Site. Conserved residues in the *β* subunit that have been proposed from the apo FTase crystal structure (*21*) to lie in the active site were investigated by site-directed mutagenesis (*22*). Of the 11 residues investigated, 5 were identified as increasing the $K_{d(FPP)}$ between 3- and 15-fold. Each of these residues (His 248*β*, Arg 291*β*, Lys 294*β*, Tyr 300*β*, and Trp 303*β*) is observed to interact with the FPP molecule in the crystal structure of the binary complex. None of the mutants investigated had an increased affinity for FPP.

Mutation of Lys 164α to asparagine causes a dramatic reduction of catalytic turnover (*36*), suggesting a direct role for this residue in catalysis. The structure of the binary complex suggests that Lys 164α may interact with the diphosphate moiety of the FPP molecule. Furthermore, its proximity to the C1 atom of FPP, which is transferred to the cysteine thiol of the CaaX substrate, is consistent with a direct role in catalysis.

Implications for Peptide Substrate Binding. The carboxy-terminal nine residues of the *β* subunit (defined as the nonapeptide) that were observed in the apo FTase crystal structure to bind in a shallow hydrophilic cleft are displaced in the binary complex. These residues may be displaced because the terminal carboxylate and Asp^1 of the nonapeptide bind in the same positively charged cleft as the diphosphate

moiety of FPP. From the crystal structure of the apoenzyme, it was hypothesized that the nonapeptide may mimic certain aspects of CaaX substrate binding (*21*). Although a CaaX peptide substrate may still bind in a portion of the hydrophilic cleft, it is clear that the carboxy-terminal residue of the nonapeptide does not mark the exact location of the terminal residue of the CaaX substrate in a ternary complex, if the observed position of FPP in the binary complex approximates its position in the ternary complex. The overall location of the bound nonapeptide observed in the apo FTase complex may, however, still mimic aspects of protein substrate binding; in particular, the interactions observed between the nonapeptide and Tyr 361β may be similar to those made with CaaX substrate molecules. Tyr 361β was involved in main-chain interactions with the nonapeptide at Asp^5 and Ser^6. This type of interaction with the main chain of CaaX substrates is reasonable since there is little specificity for the fifth or sixth residues from the carboxy terminus of these substrates. Mutation of the corresponding residue in yeast, Tyr 362β, has been shown to have an effect on peptide substrate specificity, further suggesting a direct interaction with the peptide substrate (*37*).

Additional insight into the peptide binding site may come from a recent biochemical study suggesting that Arg 202β binds the carboxy terminus of CaaX peptide substrates in a ternary complex (*22*). Mutation of this residue to alanine causes a dramatic increase in the K_m for the protein substrate Ras-CVLS and in the IC_{50} for the peptide inhibitor CVFM. Interestingly, the Arg 202β to Ala mutation showed a dramatically reduced sensitivity to CaaX-mimic inhibitors that contain the carboxy-terminal carboxylate, while inhibitors that did not contain such a carboxylate were still quite effective inhibitors of the enzyme. In the FTase−FPP complex, the position of Arg 202β is stabilized by hydrophobic interactions with the farnesyl moiety of the FPP molecule, while the guanidinium group of the residue appears to form an ion pair with Asp 200β in the FPP complex (Figure 3). Noteworthy in this regard is that mutation of Asp 200β resulted in a significant increase in the K_m for the peptide (*28*, *38*), a finding consistent with this residue's involvement in the stabilization of Arg 202β.

It is tempting to speculate that the carboxy terminus of a CaaX peptide substrate binds in a pocket near Arg 202β with a portion of the N-terminal peptide substrate binding site being formed by the hydrophilic cleft where the nonapeptide was observed to bind in the apoenzyme. In this model, the cysteine of the CaaX peptide substrate (modeled from the location of Pro^4 of the nonapeptide) would directly interact with the catalytic zinc ion, consistent with evidence that the cysteine thiol of the substrate directly coordinates the zinc ion in a ternary complex (*14*). In this position, the modeled cysteine lies between the zinc ion and the C1 atom of FPP as required for a proposed mechanism for prenyl transfer (*14*, *15*). A slight change in conformation of the first isoprene unit of FPP (C1 to C5) may occur in a ternary complex.

Molecular Ruler Hypothesis for Isoprenoid Specificity. The crystal structure of the binary complex presented here supports the mechanism of prenyl substrate specificity originally proposed from the crystal structure of FTase (*21*). The depth of the hydrophobic pocket where FPP binds is postulated to function like a molecular ruler and be the primary determinant for the specificity of the 15-carbon FPP molecule over the 20-carbon GGPP molecule, the prenyl substrate for the closely related enzyme GGTase-I. This hypothesis is supported by the observation that FPP and GGPP bind to FTase in a competitive manner but only FPP serves as an effective substrate (*10*, *13*). The bottom of the hydrophobic cavity, which marks one end of the molecular ruler, is formed by the aromatic residues Trp 102β and Tyr 205β, while the positive cleft at the top rim of the $\alpha-\alpha$ barrel near the subunit interface marks the end where the diphosphate binds. It is significant that the catalytic zinc ion binds to the rim of the $\alpha-\alpha$ barrel at the same distance from the bottom of the pocket as that of the C1 atom of the isoprenoid. A comparison of the observed location of the FPP molecule with a model of GGPP bound to FTase made by superimposing the isoprenoid moiety of GGPP on that of FPP is shown in Figure 4. While the C1 position of the observed FPP molecule is in register with the catalytic zinc ion, the C1 position of the modeled GGPP is completely out of register, preventing prenyl transfer. We hypothesize that, in the β subunit of GGTase-I, the hydrophobic cavity where its 20-carbon isoprenoid binds will be considerably deeper. This deeper cavity would allow α subunit residues Lys 164α and Tyr 200α and analogous, strictly conserved β subunit residues in the positively charged pocket to interact with the GGPP substrate similarly to the observed interactions of FTase with FPP. This molecular ruler hypothesis is consistent with the finding that, although GGPP binds to GGTase-I 330-fold more tightly than FPP, the latter can still serve as a moderately efficient substrate for this enzyme (*39*). In this regard, it may be noteworthy that overexpression of GGTase-I in *Saccharomyces cerevisiae* can rescue the growth defects of FTase null mutants, suggesting that at least in this organism GGTase-I can prenylate substrates of FTase in vivo (*40*), albeit at much reduced efficiency.

This type of mechanism for specificity in enzyme−isoprenoid interactions has also been proposed for farnesyl diphosphate synthase (FPS), which catalyzes the formation of FPP from two sequential condensation reactions of one dimethylallyl diphosphate and two isopentenyl diphosphate molecules (*41*). The crystal structure of avian FPS shows that two phenylalanine residues block the bottom of the hydrophobic cleft which binds the isoprenoid (*41*). Mutation of these residues (Phe 112 and Phe 113) results in longer prenyl diphosphate products. Furthermore, crystallographic studies of enzymes where both of these residues have been mutated reveal that the depth of the hydrophobic pocket into which the isoprenoid binds is approximately 5.8 Å deeper than that of the wild-type enzyme, supporting this mechanism of prenyl specificity (*29*).

Implications for the Design of FTase Inhibitors. A number of FPP analogues have been developed that are competitive inhibitors of FTase with respect to FPP (*42*−*45*). The selectivity of these inhibitors for FTase over other cellular enzymes, including GGTase-I, has stimulated their investigation as possible antitumor agents. The crystal structure of the binary complex of FTase with FPP presented here provides a structural framework from which to interpret the inhibitory potency of these inhibitor molecules. Among the FPP-based inhibitor molecules, the most effective retained a hydrophobic farnesyl group and a negatively charged moiety mimicking the diphosphate (*45*). For one of these

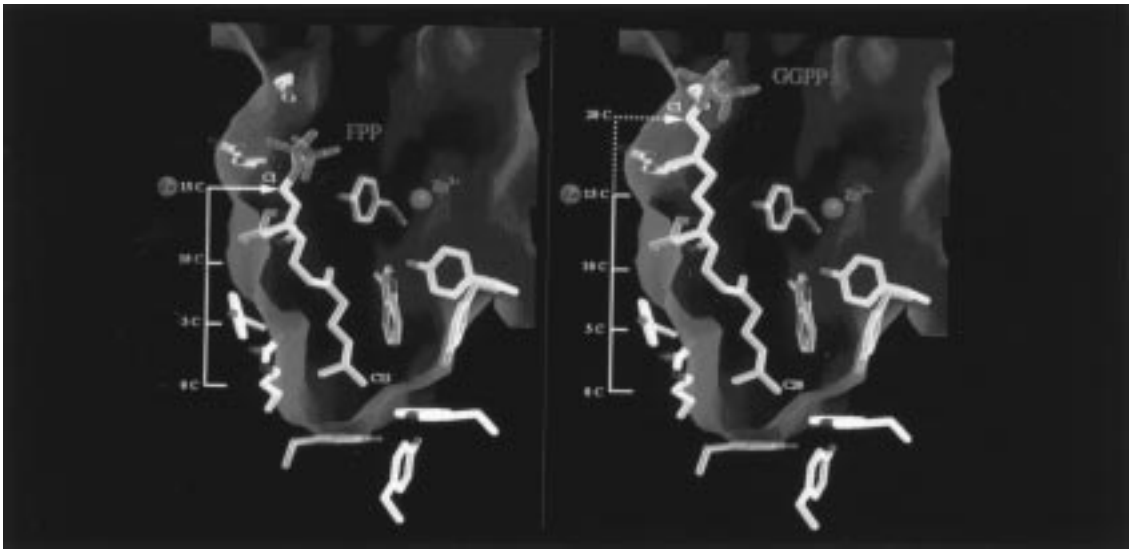

FIGURE 4: Molecular ruler hypothesis for isoprenoid substrate specificity. (Left) A portion of the solvent-accessible surface showing the observed FPP binding location. The catalytic zinc ion is in register with the C1 atom of the FPP molecule, the site of prenyl transfer. Trp 102β and Tyr 205β are at the bottom of the hydrophobic pocket. (Right) The 20 carbon long GGPP molecule, the prenyl substrate of GGTase-I, is modeled into this surface on the basis of the observed FPP location. The longer isoprenoid chain of GGPP places the C1 atom out of register with the catalytic zinc ion, accounting for the specificity of FTase for FPP over GGPP. This figure was produced with GRASP (*47*).

potent and selective FTase inhibitors [designated compound **3**, IC_{50} = 75 nM (*45*)], a systematic structure−activity analysis was carried out that indicated that the most potent inhibitors contained a terminal phosphate group rather than other types of negatively charged groups. This observation is consistent with the interactions seen with the terminal phosphate in the binary complex presented here, specifically with Tyr 300β that appears to interact with this phosphate. The length of the hydrophobic chain also had a dramatic effect on the activity in this study. Homoelongation of the farnesyl group by one carbon resulted in a decrease in IC_{50} of more than 200-fold, consistent with the crystal structure presented here and the molecular ruler hypothesis for prenyl substrate specificity.

In summary, the cocrystal structure of FTase in a binary complex with its natural substrate FPP presented here identifies the FPP binding location for this substrate and is consistent with mutagenesis data on this enzyme. The binding of FPP to FTase supports a hypothesis for prenyl substrate specificity whereby the length of the prenyl moiety is selected on the basis of the depth of the hydrophobic pocket into which it binds. This complex may provide a framework to further understand FPP-based inhibitors of FTase and may facilitate the rational design and optimization of cancer chemotherapeutic agents.

ACKNOWLEDGMENT

We thank Hee-Won Park for advice on crystallographic data collection and model refinement and thank the Keck Foundation for support of the Levine Science Research Center at Duke University.

REFERENCES

1. Zhang, F. L., and Casey, P. J. (1996) *Annu. Rev. Biochem. 65*, 241−269.
2. Schafer, W. R., and Rine, J. (1992) *Annu. Rev. Genet. 26*, 209−237.
3. Clarke, S. (1992) *Annu. Rev. Biochem. 61*, 355−386.
4. Buss, J. E., and Marsters, J. C. (1995) *Chem. Biol. 2*, 787−791.
5. Gibbs, J. B., and Oliff, A. (1997) *Annu. Rev. Pharmacol. Toxicol. 37*, 143−166.
6. Graham, S. L., and Williams, T. M. (1996) *Exp. Opin. Ther. Patents 6*, 1295−1304.
7. Reiss, Y., Goldstein, J. L., Seabra, M. C., Casey, P. J., and Brown, M. S. (1990) *Cell 62*, 81−88.
8. Moomaw, J. F., and Casey, P. J. (1992) *J. Biol. Chem. 267*, 17438−17443.
9. Moores, S. L., Schaber, M. D., Mosser, S. D., Rands, E., O'Hara, M. B., Garsky, V. M., Marshall, M. S., Pompliano, D. L., and Gibbs, J. B. (1991) *J. Biol. Chem. 266*, 14603−14610.
10. Reiss, Y., Brown, M. S., and Goldstein, J. L. (1992) *J. Biol. Chem. 267*, 6403−6408.
11. Chen, W.-J., Moomaw, J. F., Overton, L., Kost, T. A., and Casey, P. J. (1993) *J. Biol. Chem. 268*, 9675−9680.
12. Zhang, F. L., Moomaw, J. F., and Casey, P. J. (1994) *J. Biol. Chem. 269*, 23465−23470.
13. Casey, P. J., and Seabra, M. C. (1996) *J. Biol. Chem. 271*, 5289−5292.
14. Huang, C.-C., Casey, P. J., and Fierke, C. A. (1997) *J. Biol. Chem. 272*, 20−23.
15. Dolence, J. M., and Poulter, C. D. (1995) *Proc. Natl. Acad. Sci. U.S.A. 92*, 5008−5011.
16. Cassidy, P. B., and Poulter, C. D. (1996) *J. Am. Chem. Soc. 118*, 8761−8762.
17. Pompliano, D. L., Rands, E., Schaber, M. D., Mosser, S. D., Anthony, N. J., and Gibbs, J. B. (1992) *Biochemistry 31*, 3800−3807.
18. Pompliano, D. L., Schaber, M. D., Mosser, S. D., Omer, C. A., Shafer, J. A., and Gibbs, J. B. (1993) *Biochemistry 32*, 8341−8347.
19. Furfine, E. S., Leban, J. J., Landavazo, A., Moomaw, J. F., and Casey, P. J. (1995) *Biochemistry 34*, 6857−6862.
20. Tschantz, W. R., Furfine, E. S., and Casey, P. J. (1997) *J. Biol. Chem. 272*, 9989−9993.
21. Park, H.-W., Boduluri, S. R., Moomaw, J. F., Casey, P. J., and Beese, L. S. (1997) *Science 275*, 1800−1804.
22. Kral, A. M., Diehl, R. E., deSolms, S. J., Williams, T. M., Kohl, N. E., and Omer, C. A. (1997) *J. Biol. Chem. 272*, 27319−27323.
23. Fu, H.-W., Beese, L. S., and Casey, P. J. (1998) *Biochemistry 37*, 4465−4472.

24. Reiss, Y., Seabra, M. C., Armstrong, S. A., Slaughter, C. A., Goldstein, J. L., and Brown, M. S. (1991) *J. Biol. Chem. 266*, 10672−10677.
25. Bukhtiyarov, Y. E., Omer, C. A., and Allen, C. M. (1995) *J. Biol. Chem. 270*, 19035−19040.
26. Yokoyama, K., McGeady, P., and Gelb, M. H. (1995) *Biochemistry 34*, 1344−1354.
27. Ying, W., Sepp-Lorenzino, L., Cai, K., Aloise, P., and Coleman, P. S. (1994) *J. Biol. Chem. 269*, 470−477.
28. Dolence, J. M., Rozema, D. B., and Poulter, C. D. (1997) *Biochemistry 36*, 9246−9252.
29. Tarshis, L. C., Proteau, P. J., Kellogg, B. A., Sacchettini, J. C., and Poulter, C. D. (1996) *Proc. Natl. Acad. Sci. U.S.A. 93*, 15018−15023.
30. Otwinowski, Z., and Minor, W. (1997) *Methods Enzymol. 276A*, 307−326.
31. Brunger, A. T. (1992) in *X-PLOR version 3.1: A System for X-ray Crystallography and NMR*, Yale University Press, New Haven, CT.
32. Brunger, A. T., and Jiang, J. S. (1994) *J. Mol. Biol. 243*, 100−115.
33. Jones, T. A., and Kjeldgaard, M. (1993) in *O version 5.9, The manual*, Uppsala University, Uppsala, Sweden.
34. CCP4 (1994) *Acta Crystallogr. D50*, 760.
35. Wallace, A., Koblan, K. S., Hamilton, K., Marquis-Omer, D. J., Miller, P. J., Mosser, S. D., Omer, C. A., Schaber, M. D., Cortese, R., Oliff, A., Gibbs, J. B., and Pessi, A. (1996) *J. Biol. Chem. 271*, 31306−31311.
36. Andres, D. A., Goldstein, J. L., Ho, Y. K., and Brown, M. S. (1993) *J. Biol. Chem. 268*, 1383−1390.
37. Villar, K. D., Mitsuzawa, H., Yang, W., Sattler, I., and Tamanoi, F. (1997) *J. Biol. Chem. 272*, 680−687.
38. Omer, C. A., Kral, A. M., Diehl, R. E., Prendergast, G. C., Powers, S., Allen, C. M., Gibbs, J. B., and Kohl, N. E. (1993) *Biochemistry 32*, 5167−5176.
39. Yokoyama, K., Zimmerman, K., Scholten, J., and Gelb, M. H. (1997) *J. Biol. Chem. 272*, 3944−3952.
40. Trueblood, C. E., Ohya, Y., and Rine, J. (1993) *Mol. Cell. Biol. 13*, 4260−4275.
41. Tarshis, L. C., Yan, M., Poulter, C. D., and Sacchettini, J. C. (1994) *Biochemistry 33*, 10871−10877.
42. Manne, V., Ricca, C. S., Brown, J. G., Tuomari, A. V., Yan, N., Patel, D., Schmidt, R., Lynch, M. J., Ciosek, C. P., Jr., Carboni, J. M., Robinson, S., Gordon, E. M., Barbacid, M., Seizinger, B. R., and Biller, S. A. (1995) *Drug Dev. Res. 34*, 121−137.
43. Gibbs, J. B., Pompliano, D. L., Mosser, S. D., Rands, E., Lingham, R. B., Singh, S. B., Scolnick, E. M., Kohl, N. E., and Oliff, A. (1993) *J. Biol. Chem. 268*, 7617−7620.
44. Cohen, L. H., Valentijn, A. R. P. M., Roodenburg, L., Van Leeuwen, R. E. W., Huisman, R. H., Lutz, R. J., Van Der Marel, G. A., and Van Boom, J. H. (1995) *Biochem. Pharmacol. 49*, 839−845.
45. Patel, D. V., Schmidt, R. J., Biller, S. A., Gordon, E. M., Robinson, S. S., and Manne, V. (1995) *J. Med. Chem. 38*, 2906−2921.
46. Carson, M. (1987) *J. Mol. Graphics 5*, 103−106.
47. Nicholls, A. (1992) in *GRASP: Graphical Representation and Analysis of Surface Properties*, Columbia University Press, New York, NY.

BI980708E